# Electronic supporting information (ESI)

## Low-temperature electronic transport of manganese silicide shell-protected single crystal nanowires for nanoelectronics applications

*Alexsandro dos Santos E. da Cruz,*[a]* *Marcos V. Puydinger dos Santos,*[a] *Raul B. Campanelli,*[a] *Pascoal G. Pagliuso,*[a] *Jefferson Bettini,* [b] *Kleber R. Pirota,*[a] and *Fanny Béron*[a]

[a]Institute of Physics Gleb Wataghin (IFGW), University of Campinas (UNICAMP), Campinas, 13083-859 São Paulo, Brazil

[b]Brazilian Center for Research in Energy and Materials (CNPEM), Brazilian Nanotechnology National Laboratory (LNNano), Campinas, 13085-903 São Paulo, Brazil

* Corresponding author

asec@ifi.unicamp.br

### *Suppl. 1 – Nanowire diameter variation*

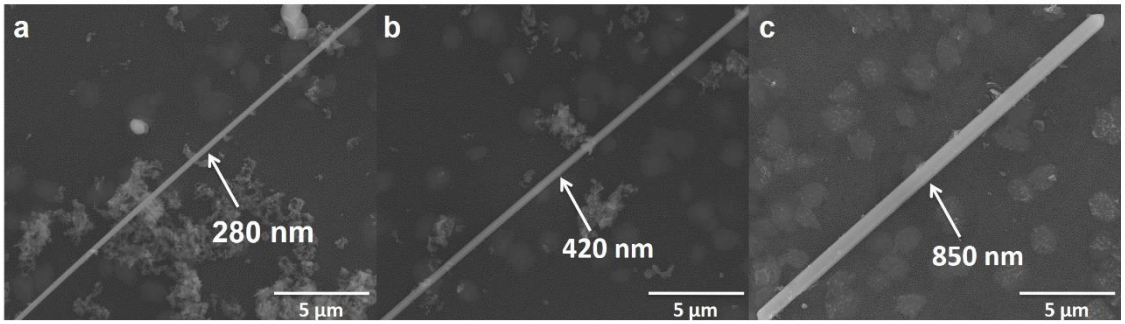


**Fig. S1** Nanowire diameter. SEM images of different nanowires, with diameters larger than the alumina template pores. (a) $d$ = 280 nm, (b) $d$ = 420 nm, and (c) $d$ = 850 nm.

### *Suppl. 2 – Energy dispersive X-Ray spectroscopy (EDS)*

Before the EDS spectrum analyses, we calibrated the equipment with Cu-K$\alpha_1$ and C-K$\alpha_1$ energies from standards. The spectrum shown in Fig. S2 summarizes all the observed elements including Mn-K$\alpha_{1,2}$ (5.9 keV), Mn-K$\beta_1$ (6.4 keV), Mn-L$\alpha_1$ (0.6 keV),

Si-K$\alpha_{1,2}$ (1.7 keV), Si-K$\beta_1$ (1.8 keV), O-K$\alpha_{1,2}$ (0.5 keV), Ga-K$\alpha_{1,2}$ (9.2 keV), Ga-K$\beta_1$ (10.2 keV), and Ga-L$\alpha_1$ (1.1 keV) edges.[1] Additionally, the C-K$\alpha_1$ (0.2 keV), Cu-K$\alpha_{1,2}$, (8.0 keV), -K$\beta_1$ (8.9 keV) and Cr-K$\alpha_{1,2}$ (5.4 keV), -L$\alpha_1$ (0.5 keV) edges were also observed. The edges from C and Cu are expected to originate from the carbon thin film covering the copper grid used for the TEM. The third additional element (Cr) was found in a low atomic concentration (≈ 0.7 at.%), which is below the typical concentration error of EDS (around 2 at.%). Therefore, we have excluded it from our analysis since we did not use any Cr source in our synthesis. The Cr-Kα signal is likely to be a sum peak from three Si-Kα (1.74 keV) X-ray photons that arrived simultaneously at the detector, thus impeding their distinction by the pulse processor.

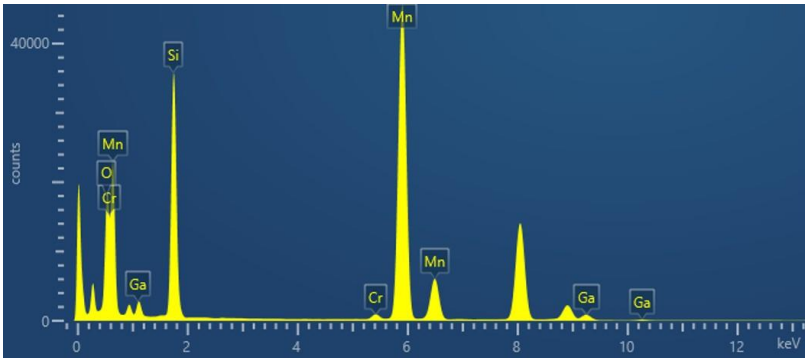


**Fig. S2** EDS spectrum of area 2.

EDS spectra were carried out on six different areas along the length of a 7 µm-long nanowire (Fig. S3). The EDS mapping was then performed and the results are presented in Figs. S4-S8 along with the element intensity scan, while those from area 3 are shown in Fig. 2. A core-shell structure is present throughout the nanowire length. The core consists of Mn and Si, whereas the bilayer shell is assumed to be composed of $Ga_2O_3$ and $SiO_2$ as they are the most stable oxides for these elements.

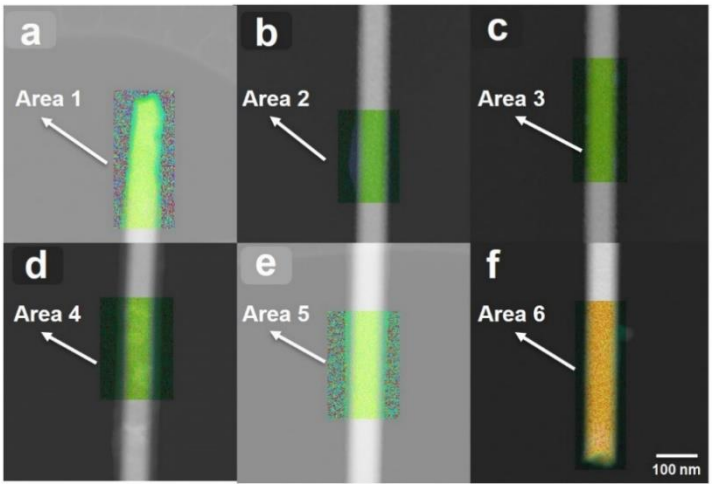


**Fig. S3** EDS mapping probed areas. (a)-(f) Rectangular areas probed by EDS along the nanowire length. Area 3 is the region shown in Fig. 2.

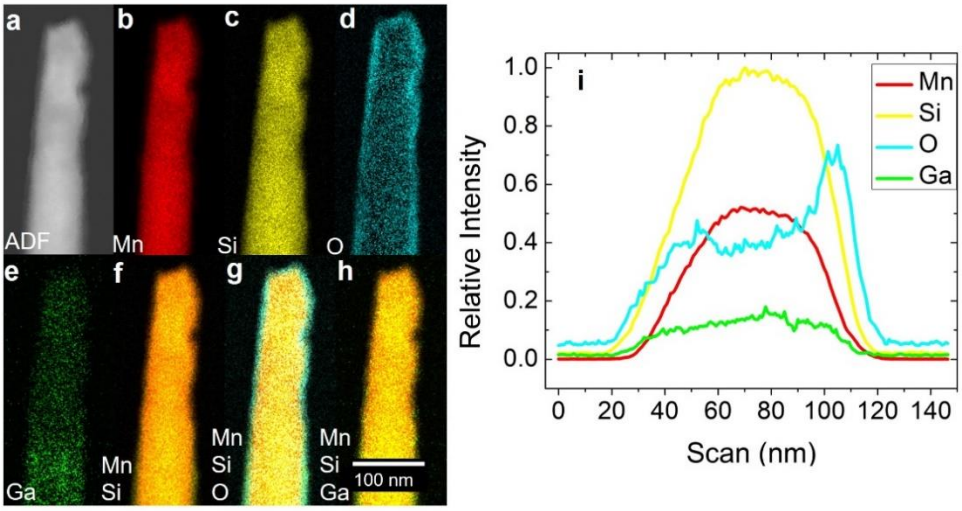


**Fig. S4** Area 1 Cf Fig. 2.

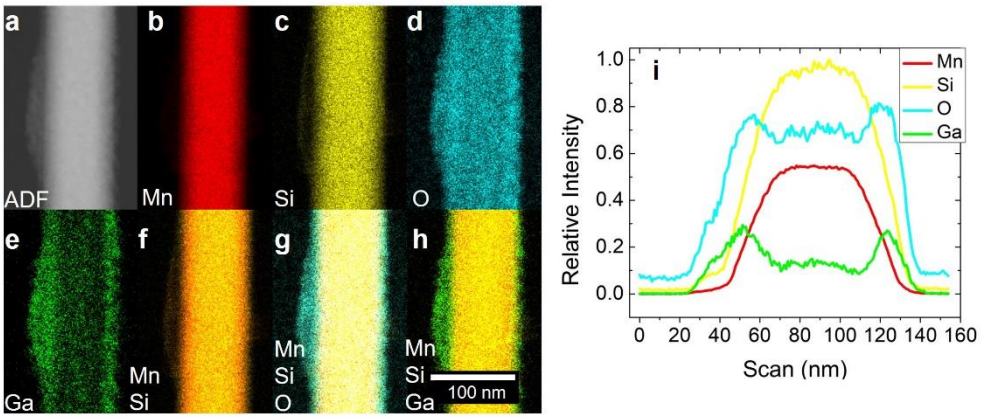


**Fig. S5** Area 2 Cf Fig.2.

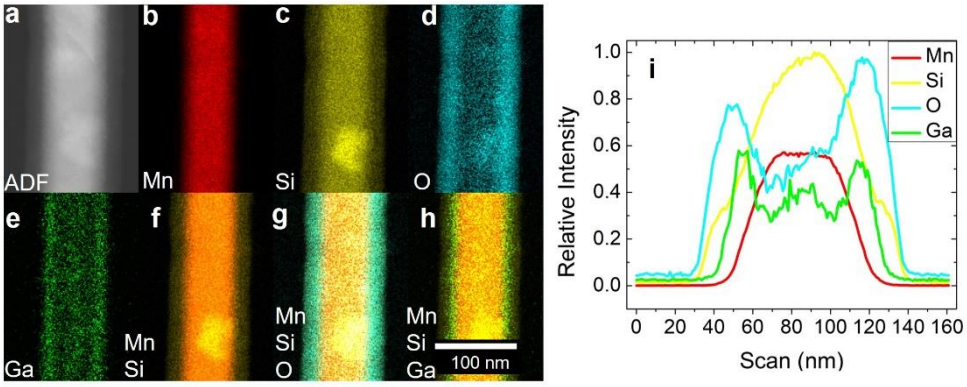


**Fig. S6** Area 4 Cf Fig.2.

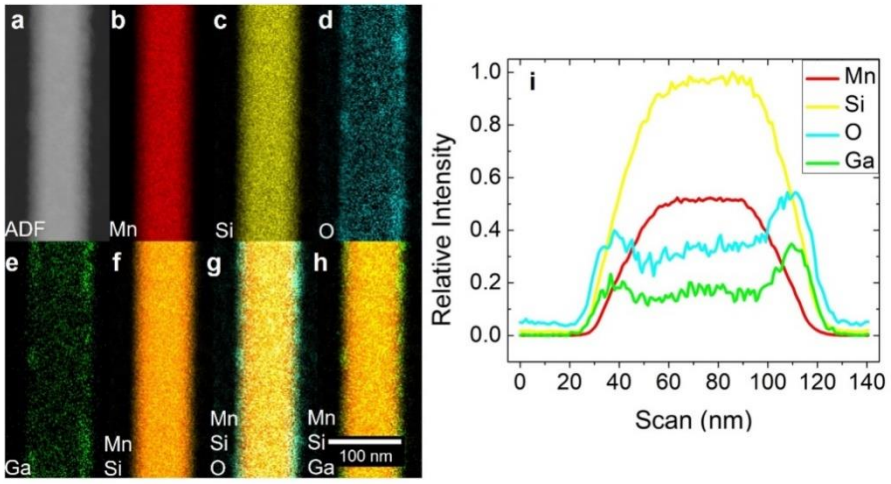


**Fig. S7** Area 5 Cf Fig.2.

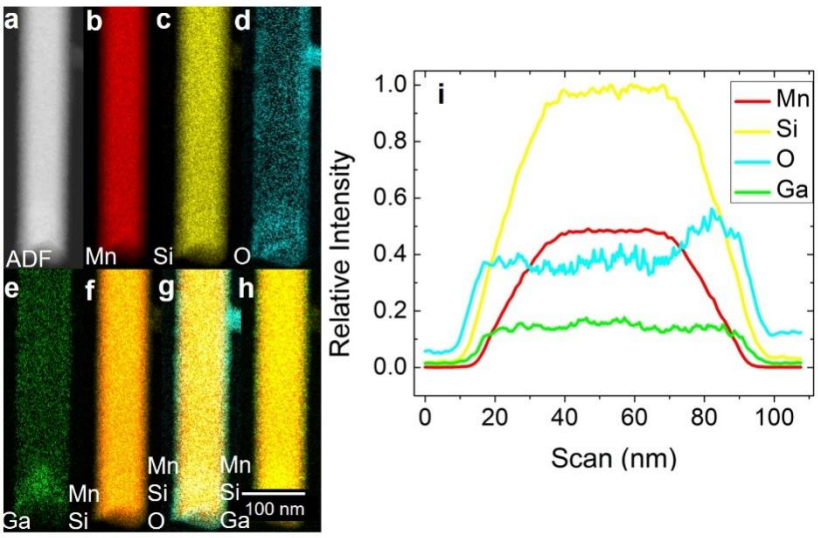


**Fig. S8** Area 6 Cf Fig.2.

***Core composition***

The proportional signal obtained by EDS between Mn and Si can yield misleading conclusions as the Si characteristic X-rays come from either the Mn-Si core or the $SiO_2$ shell. Therefore, to obtain a more reliable proportion of the core composition, we subtracted the Si contribution from the EDS signal as explained below:

The measured Mn concentration, $C_{Mn}$, is given by:[2]

$$C_{Mn} = \frac{A_{Mn}}{A_{Mn} + A_{Si}^{Core} + A_{Si}^{Shell}} \qquad (S1)$$

where $A_{Si}^{Core}$ and $A_{Si}^{Shell}$ are the Si core and shell areas, respectively, and $A_{Mn} = A_{Mn}^{Core}$ is the Mn core area. However, the Mn desired concentration should only take into account the Si from the core, leading to:

$$C_{Mn}^{*} = \frac{A_{Mn}}{A_{Mn} + A_{Si}^{Core}} \qquad (S2)$$

We should note that the Si core ($A_{Si}^{Core}$) and Mn ($A_{Mn}$) areas are exactly the same, which gives:

$$C_{Mn}^{*} = C_{Mn} + C_{Mn}\frac{A_{Si}^{Shell}}{2\,A_{Si}^{Core}} \qquad (S3)$$

From the corrected atomic percentages, after the area correction given by Eq. S3, the Mn and Si concentrations in the nanowire core are 63 and 37 at.%, respectively (Table S1).

**Table S1.** Mn and Si corrected concentrations in the nanowire core.

| | **Mn (at. %)** | **Si (at. %)** |
|---|---|---|
| **Area 1** | 69.9 | 30.1 |
| **Area 2** | 60.3 | 39.7 |
| **Area 3** | 59.7 | 40.3 |
| **Area 4** | 61.6 | 38.4 |
| **Area 5** | 63.4 | 36.6 |
| **Area 6** | 65.8 | 34.2 |
| **Average** | 63.4 | 36.6 |

***Suppl. 3 – Selected area electron diffraction (SAED)***

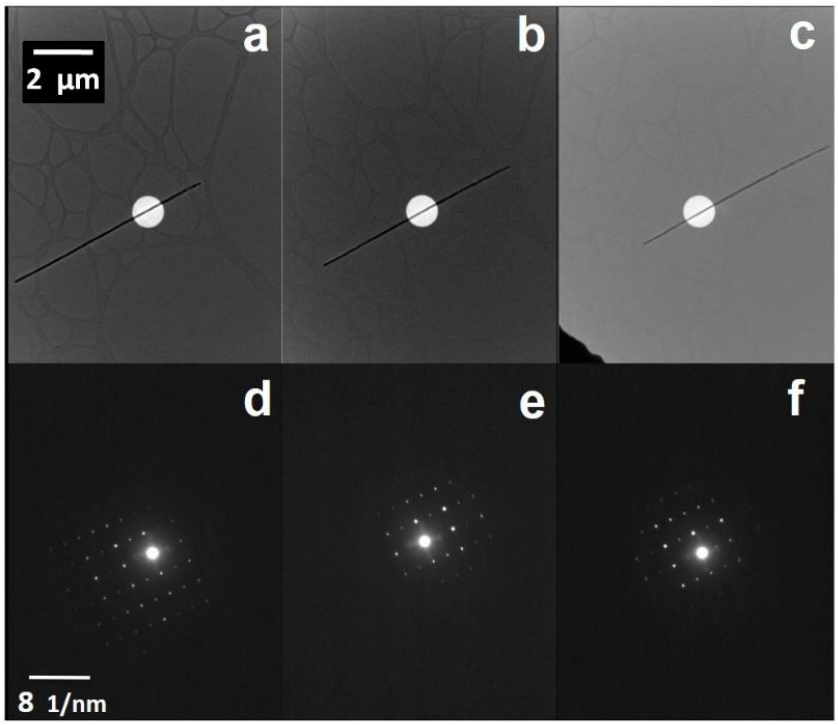


**Fig. S9** SAED patterns along the nanowire. (a)-(c) Nanowire images with the microscope aperture (white circle) and (d)-(f) respective SAED patterns taken at the [210] zone axis.

***Suppl. 4 – Transmission Kikuchi diffraction (TKD)***

In the pole figures, we only observe some discrete regions rather than a continuous color change on the globe surfaces (Fig. S10a). These spots arise from the scattered electrons in the Bragg condition, demonstrating that the probed nanowire has neither texture nor other precipitated phases or grains in different orientations. To reinforce the aforementioned observation, a secondary electron and other TKD image types are shown in Fig. S10b. First, we only see a single gray tone in the band contrast, indicating the absence of grain boundaries as they would appear as black lines. Second, the inverse pole map, which is sensitive to the grain orientations, exhibits a homogenous color for each direction. This suggests that the same orientation persists throughout the nanowire length. For a similar reason, Euler map analysis comforts this conclusion, as each set of Euler angles ($\Phi_1$, $\theta$, $\Phi_2$) would change color. Finally, the absence of phase-contrast difference (red map) indicates a homogeneous nanowire composition throughout its length.

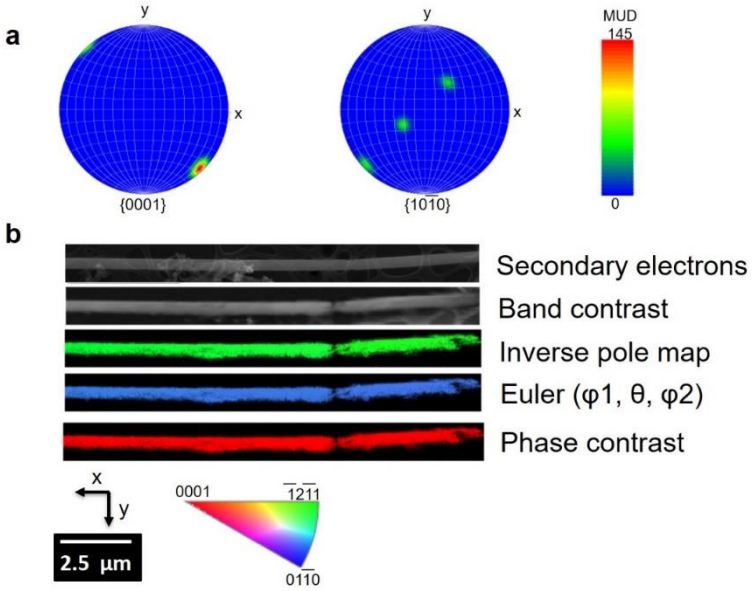


**Fig. S10** TKD analysis. (a) Pole figures representing the scattered electron beam in specific directions. (b) Secondary electron image and TKD maps indicating the nanowire microstructure.

### *Suppl. 5 – Sample preparation for transport measurements*

The four-probe platinum (Pt) electrodes used for transport measurements were prepared on a Si substrate covered by a thermally-grown $SiO_2$ layer using standard optical lithography with 405 nm wavelength in a Karl Süss mask aligner MJB3. The electrodes are formed by six free connections, of which four have been used for the resistivity measurements (Fig. S11).

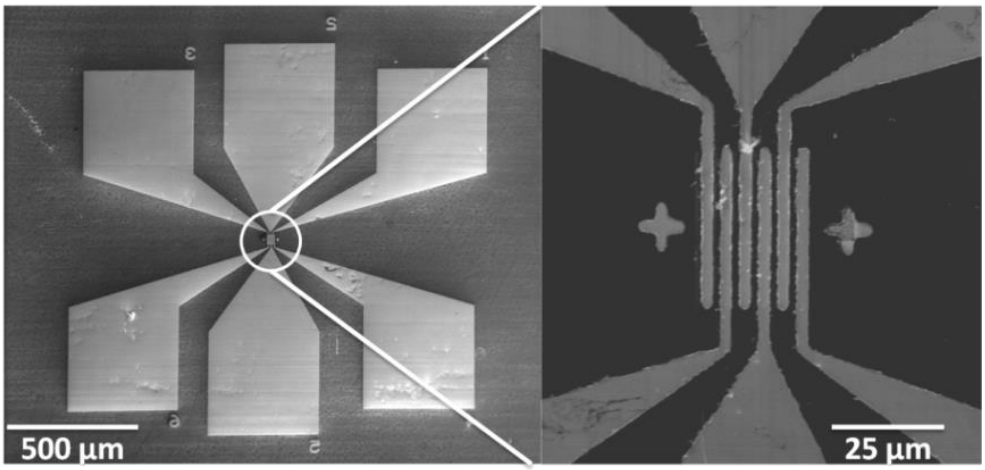


**Fig. S11** Electrical transport platform. Top view of the Pt electrodes used for the nanowire resistivity measurements.

The individual nanowires were moved from the alumina template surface to the platinum electrodes using a nanomanipulator in a Helios 660 focused ion beam (FIB) system. However, the presence of a 12 nm-thick oxide layer may impair the current input through the nanowires. Therefore, we employed a thinning process using the FIB tool to remove this oxide layer and adequately probe their electrical resistivity. Firstly, we impinged 30 keV $Ga^+$ ions at a 10 pA current into the top oxide layer, as a milling process to expose the Mn-Si core. A focused-ion-beam-induced deposition (FIBID) of platinum carbon was then performed using a similar 30 keV $Ga^+$ ion beam with a 10pA current to contact the nanowire core with the electrodes. We chose an ion beam rather than an electron one to deposit the platinum-carbon layer once the typical metal content deposited is around 19-30 at.% Pt, against 11-17 at.% in the case of focused electron-beam-induced deposition (FEBID).[3] This process is exemplified in Fig. S12.

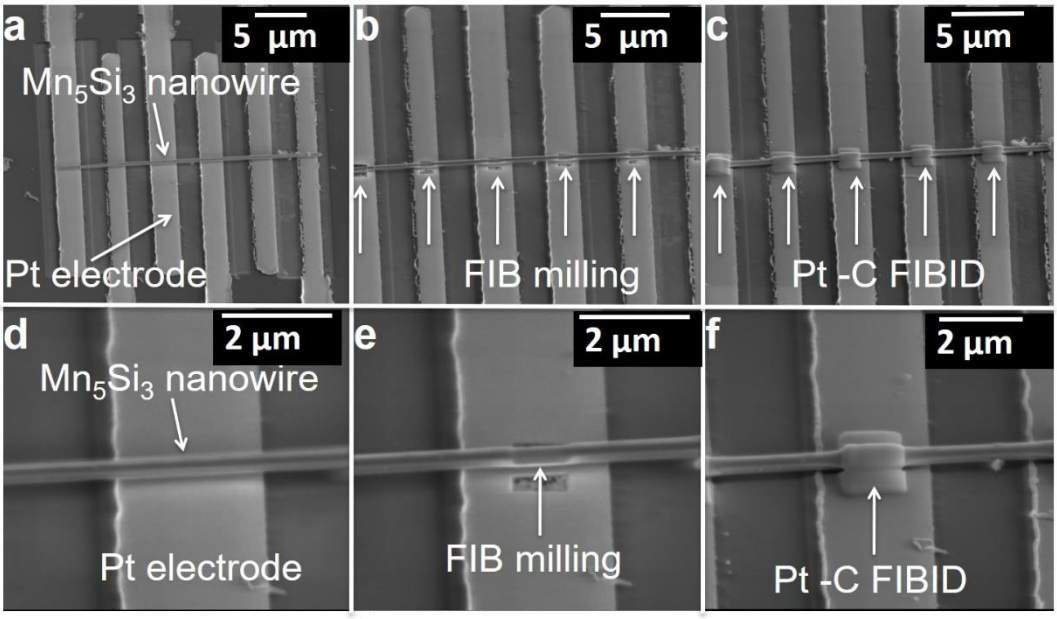


**Fig. S12** Contact process. (a)-(c) Global view. (d)-(f) Zoom on one contact. (a), (d) Nanowire deposited on the electrode using the FIB nanomanipulator. (b), (e) After the FIB milling to remove the oxide layer. (c), (f) After the Pt-C deposition to contact the nanowire with the electrodes.

Finally, the ohmic contact nature was verified before carrying out the nanowire resistance ($R$) measurements. Typical results are presented in Fig. S13, where a current ($I$) vs voltage ($V$) linear behavior is obtained when performing the standard four-probe measurement with an applied current amplitude of 0.8 $\mu$A at 2 and 300 K on a 450 nm diameter nanowire, indicating the achievement of an ohmic electric contact. Therefore,

the sample preparation was successfully performed, which allows us to probe the nanowires through electrical measurements in the temperature ($T$) range of 2-300 K. The measurements were carried out during cooling experiments with a 1 K step. Each data point is the average of two resistance measurements at the same temperature.

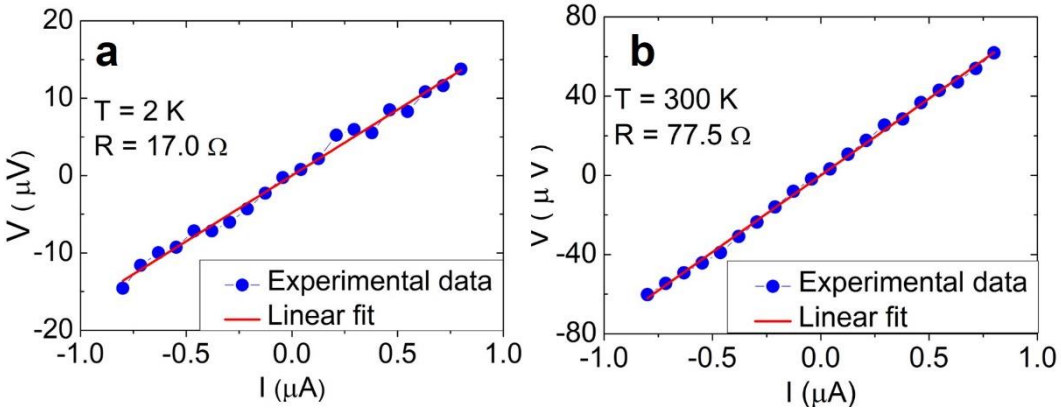


**Fig. S13** Ohmic contact. Representative $I$ x $V$ curves at (a) 2 and (b) 300 K for 450 nm diameter nanowire.

### *Suppl. 6 – Resistivity curve linearization*

To perform the data linearization, we applied the natural logarithm to extract the power law in a given temperature range. Since the noise is detrimental to the fitting, the data below 11 K were excluded for all samples. Fig. S14 shows the fit quality parameter, $\boldsymbol{\chi^2}$, for the resistivity linearization of the nanowires of 180, 450, and 800 nm in diameter. Although they all are near to 1, indicating a good fit quality, the largest nanowire presents the lowest value. Its curve is noisier than the others, which may explain the gap observed between the end of the magnon-electron temperature range and the beginning of the phonon resistivity contribution for this particular sample. In the lower temperature range, the magnon-electron was found to be the main scattering process for the diameter of 180, 450, and 800 nm as they present $\boldsymbol{n}$ = 2.0 ± 0.1, 2.0 ± 0.1, and 1.9 ± 0.1, respectively. At higher temperatures, the smallest nanowire is the only one that does not turn into a phonon scattering process since $\boldsymbol{n}$ is equal to 1.3 ± 0.1, while both larger diameters present 1.1 ± 0.1.

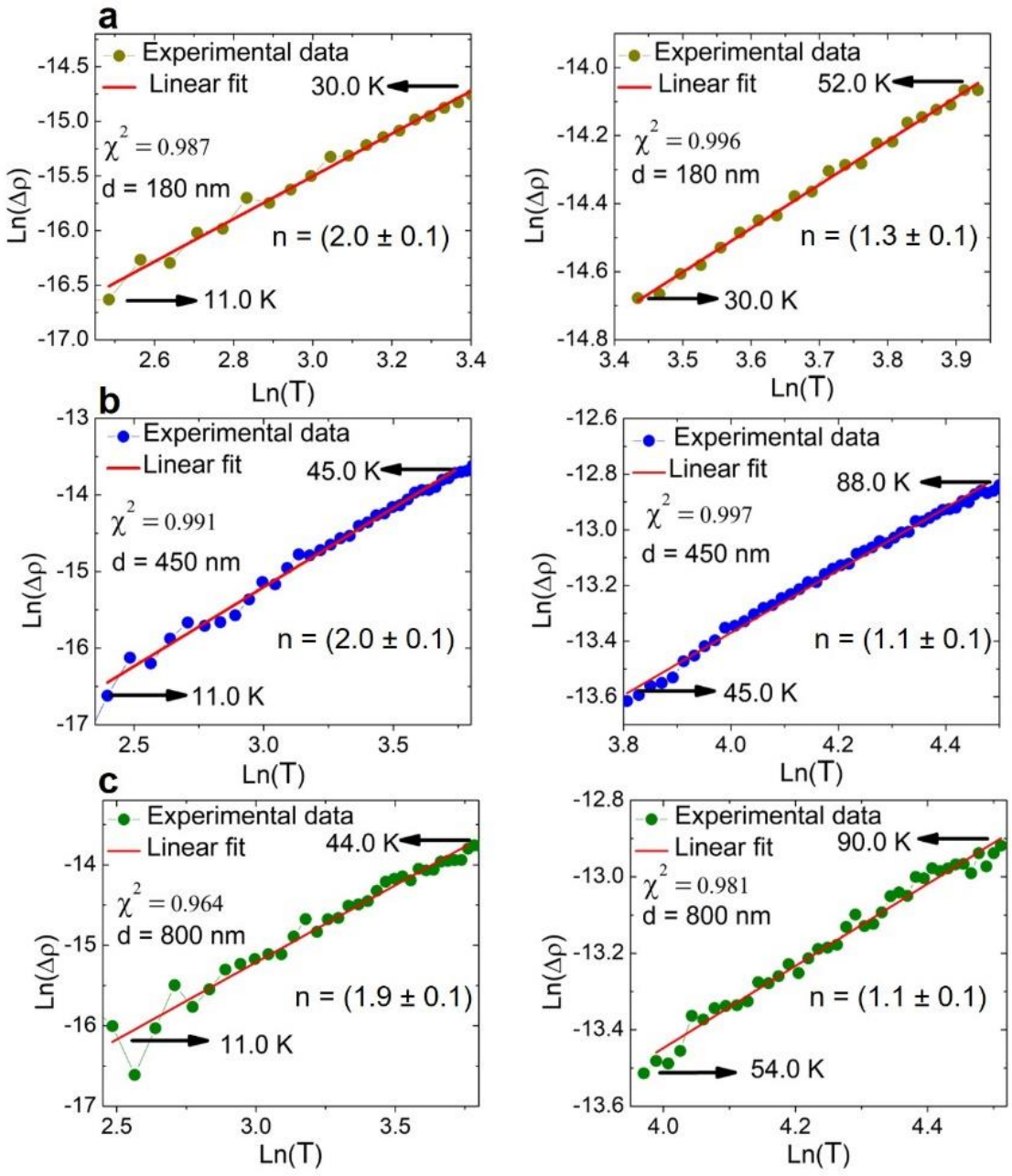


**Fig. S14** Resistivity data linearization. Lower temperature (left) and higher temperature (right) intervals presenting a linear behavior for diameters of (a) 180 nm, (b) 450 nm, and (c) 800 nm.

## References


1 A. Thompson, D. Attwood, E. Gullikson, M. Howells, K.-J. Kim, J. Kirz, J. Kortright, I. Lindau, Y. Liu, P. Pianetta, A. Robinson, J. Scofield, J. Underwood, G. Williams and H. Winick, *Lawrence Berkeley Natl. Lab.*, 2009.

2 W. D. Callister, *Materials science and engineering: An introduction*, John Wiley & Sons, 2nd edn., 1991.

3 J. M. De Teresa, R. Córdoba, A. Fernández-Pacheco, O. Montero, P. Strichovanec and M. R. Ibarra, *J. Nanomater.*, 2009, **2009**, 1–11.